

Two-dimensional hybrid composites of SnS_2 with graphene and graphene oxide for improving sodium storage: A first-principles study

Kum-Chol Ri^a, Chol-Jun Yu^{*a}, Jin-Song Kim^a, Song-Hyok Choe^a

^aChair of Computational Materials Design, Faculty of Materials Science, Kim Il Sung University, Ryongnam-Dong, Taesong District, Pyongyang, Democratic People's Republic of Korea

Abstract

Among the recent achievements of sodium-ion battery (SIB) electrode materials, hybridization of two-dimensional (2D) materials is one of the most interesting appointments. In this work, we propose to use the 2D hybrid composites of SnS_2 with graphene or graphene oxide (GO) layers as SIB anode, based on the first-principles calculations of their atomic structures, sodium intercalation energetics and electronic properties. The calculations reveal that graphene or GO film can effectively support not only the stable formation of hetero-interface with the SnS_2 layer but also the easy intercalation of sodium atom with low migration energy and acceptable low volume change. The electronic charge density differences and the local density of state indicate that the electrons are transferred from the graphene or GO layer to the SnS_2 layer, facilitating the formation of hetero-interface and improving the electronic conductance of the semiconducting SnS_2 layer. These 2D hybrid composites of SnS_2/G or GO are concluded to be more promising candidates for SIB anodes compared with the individual monolayers.

Key words: Sodium-ion battery, Anode, Tin oxide, Graphene oxide, First-principles method

1. Introduction

Recently, inorganic two-dimensional (2D) materials have attracted remarkable attention for various energy applications including energy harvesting and energy storage devices due to their unique structural and electrochemical properties [1, 2, 3, 4]. Graphene and chemically modified graphene such as graphene oxide (GO) or reduced graphene oxide (rGO) are regarded as the representative 2D materials, being characterized by layer-stacked structures coupled by weak interlayer van der Waals (vdW) and strong in-plane covalent bonding interactions [5, 6, 7, 8, 9]. Such graphene-like 2D structures can be found in elemental analogues of graphene (silicene, germanene, phosphorene, borophene), transition metal oxides (TMOs) [10], transition metal dichalcogenides (TMDs) [11, 2, 12], and transition metal carbides/nitrides (MXenes) [13]. These 2D materials can be obtained by exfoliation or synthesis, and can provide large surface area with abundant anchoring sites and low volume change during the de/intercalation processes of atoms or molecules. Therefore, 2D materials can be used as potential electrode materials for alkali-ion batteries with remarkably large capacity, high rate capability, good cycle performance and low price.

Many of 2D materials such as rGO [14, 15, 16], layered vanadium pentoxide (V_2O_5) [17] and molybdenum disulfide (MoS_2) [18] have been verified to be used as efficient electrode materials for lithium-ion batteries (LIBs) and sodium-ion batteries (SIBs) by experimental and theoretical studies. In fact,

as the most widely used and standard anode material for LIBs, graphite has the theoretical capacity of $372 \text{ mA}\cdot\text{h}\cdot\text{g}^{-1}$, which is not high enough to satisfy the growing demand of battery capacity. For SIBs, moreover, it is almost impossible to intercalate sodium itself into graphite due to a big mismatch between the ionic radius of Na^+ cation and the interlayer distance of graphite, and thus co-intercalation with organic molecules has been devised [19, 20, 21]. Alternatively, graphene and its derivatives such as GO or rGO, which can be obtained by exfoliation from graphite, have been studied extensively, confirming the doubled capacity compared with graphite, very high surface area ($2680 \text{ m}^2\cdot\text{g}^{-1}$), high electron conductivity and excellent chemical stability [14, 22, 23, 15, 16]. However, both Li and Na bind very weakly to the pristine graphene or GO, resulting in Li/Na clustering and dendrite growth. On the other hand, tin disulfide (SnS_2) as the typical TMD is recognized as a promising anode material due to its high initial capacity with an unique mechanism of alkali cation storage reaction [24, 25, 26]. The bulk SnS_2 has PbI_2 -type layered structure and exhibits a high lithium storage capacity (average capacity $583 \text{ mA}\cdot\text{h}\cdot\text{g}^{-1}$ after 30th cycles) and a good cycling stability (cycle life performance 85% after 30 cycles) [25], being much better performance than the conventional graphite electrodes. The lithium or sodium storage in SnS_2 is performed through the two-step reactions; (1) conversion of SnS_2 into metallic Sn and (2) alloying with lithium or sodium forming Li-Sn or Na-Sn alloy. By contrast, only the conversion reaction occurs during the lithium or sodium storage in other TMDs such as MoS_2 , WS_2 and VS_2 [12]. The reversible alloying reaction was found to give a large capacity of sodium storage in the first cycle, but to be accompanied with a large volume expansion (e.g., 420% for

*Corresponding author

Email address: c.j.yu@ryongnamsan.edu.kp (Chol-Jun Yu)

the case of Na-Sn alloying [27, 28]), leading to a poor capacity after a few cycles.

Designing hetero-layered architectures by coupling graphene or GO with TMD or TMO 2D materials has emerged as an effective strategy to enhance the Li/Na binding strength and reduce the volume change as well [29, 30, 31, 32]. In particular, the hybrid composites formed by coupling rGO and TMDs have been reported to show a good performance as anode materials for LIBs and SIBs [33, 34, 35]. In such composite systems, graphene-based 2D materials can not only serve as a matrix to anchor the TMD layers but also improve the electrochemical performance of semiconducting TMDs. As a typical example of such composites, therefore, the hybrid SnS_2/rGO composites including the hetero-interface can be constructed and used as excellent anode materials by combining the metallic electrical conductivity of graphene with the high storage capability of SnS_2 [36, 37, 38, 39, 40, 41]. These synthesized SnS_2/rGO hybrids have shown to exhibit the excellent electrochemical performance such as high sodium storage capacity of $649 \text{ mA}\cdot\text{h}\cdot\text{g}^{-1}$ at the current density of $100 \text{ mA}\cdot\text{g}^{-1}$, ultra-long cycle life of 89% and 69% after 400 and 1000 cycles, and superior rate capability of $337 \text{ mA}\cdot\text{h}\cdot\text{g}^{-1}$ at the higher current density of $12.8 \text{ A}\cdot\text{g}^{-1}$ (28C) in only 1.3 minutes [37, 38, 39, 40]. To the best of our knowledge, no theoretical works for 2D hybrid SnS_2/G or GO composites can be found in literature in spite of such successful experiments and the great importance of clarifying the operational mechanism, motivating us to investigate these hetero-interfaces in atomic scale by means of first-principles modeling and simulations.

In this work, we make a modeling of hybrid SnS_2/G and SnS_2/GO composites, together with 2D bilayered SnS_2 , for conducting comparative and systematic study by using first-principles calculations within the density functional theory (DFT). Performing the structural optimizations, we analyze the detailed atomic structures of these 2D layered compounds, such as interlayer distance and bond lengths. The activation barriers for the in-plane atomic migrations of sodium atom are calculated in these composite systems of SnS_2/G and SnS_2/GO , and in the SnS_2 bilayer. The local density of states (LDOS) and electronic charge density differences are analyzed. Based on the calculation data, we reveal the crucial role of hetero-interface behind the Na-storage enhancement of SnS_2/GO hybrid.

2. Computational Methods

Regarding the atomistic modeling, three kinds of 2D systems, *i.e.*, SnS_2 , SnS_2/G and SnS_2/GO , were built using the corresponding supercells. The SnS_2 crystal has the hexagonal structure ($P\bar{3}m1$ space group) with the lattice constants of $a = 3.649 \text{ \AA}$ and $c = 5.899 \text{ \AA}$ [42], characterized by the interlayer stacking called 2H- SnS_2 polytype as recently studied with first-principles method [43, 44, 45, 46]. For modeling of the SnS_2 layer, we used a AA-stacked SnS_2 bilayer, employing the hexagonal (2×2) cells in plane, which contain 4 Sn atoms and 8 S atoms in one layer. For the composite systems of SnS_2 layer with graphene or GO layer, we built sandwiched supercells, where the SnS_2 bilayer is placed in between the graphene

or GO layers, giving the hybrid SnS_2/G or SnS_2/GO composite. Again, the hexagonal (2×2) cells were used for modeling of SnS_2 bilayer in these composite systems, while the AA-stacked hexagonal (3×3) cells were employed for the graphene or GO layer that contains 18 C atoms or 18 C atoms and 9 O atoms in one layer. It should be noted that the GO layer with the C/O atomic ratio of 2:1 was formed by decorating epoxy groups ($-\text{O}-$) on outer side of the graphene sheet. For these supercell models, fixed cell lengths of $a = b = 7.79 \text{ \AA}$ and $c = 30 \text{ \AA}$ were used throughout the work, providing the vacuum layer thickness over 15 \AA (see Figure S1).

All the calculations in this work were carried out using the pseudopotential plane-wave method as implemented in QUANTUM ESPRESSO package (version 6.2) [47]. We utilized the projector augmented wave (PAW) method to describe the interaction between ions and valence electrons¹. The PBEsol functional [48] within the generalized gradient approximation (GGA) was used for the exchange-correlation interaction between valence electrons. To take into account the vdW interaction between the layers, the vdW energy provided by the exchange-hole dipole moment (XDM) method [49] was added to the DFT total energy. As the major computational parameters, plane-wave cutoff energies were set to be 40 Ry for wave function and 400 Ry for electron density, and the Monkhorst-Pack special k -points were set to be ($4 \times 4 \times 1$) for all the supersell models, providing a total energy accuracy of 5 meV per atom. Self-consistent convergence threshold for total energy was 10^{-9} Ry, and the convergence threshold for atomic force in structural relaxations was $4 \times 10^{-4} \text{ Ry}\cdot\text{Bohr}^{-1}$. Fermi-Dirac function with a gaussian spreading factor of 0.01 Ry was applied to the Brillouin-zone integration.

To calculate the activation barriers for sodium migration, we applied the climbing image nudged elastic band (NEB) method [50]. During the NEB runs, the supercell dimensions were fixed, while all the atomic positions were allowed to relax until the atomic forces converge within $0.05 \text{ eV}\cdot\text{\AA}^{-1}$. The number of NEB images was tuned so that the distance between neighbouring NEB images was less than 1 \AA . We used the image energies and their derivatives to make an interpolation of the path energy profile that passes through every image points, as implemented in the `neb.x` code of QUANTUM ESPRESSO package [47].

In order to estimate the binding strength between the layers, we calculated the interlayer binding energy per atom as follows [20, 21],

$$E_b = \frac{1}{N} [E(d = d_{\text{eq}}) - E(d = d_{\infty})] \quad (1)$$

where $E(d = d_{\text{eq}})$ and $E(d = d_{\infty})$ are the DFT total energies of the supercells with the interlayer distance at equilibrium (d_{eq}) and infinity (d_{∞}), respectively, and N is the number of atoms included in the supercell. Due to the numerical limitation, d_{∞} was approximated to be $\sim 15 \text{ \AA}$, over which the total energy of

¹We used C.pbesol-n-kjpaw_psl.0.1.UPF, O.pbesol-n-kjpaw_psl.0.1.UPF, Sn.pbesol-dn-kjpaw_psl.0.2.UPF, S.pbesol-n-kjpaw_psl.0.1.UPF, and Na.pbesol-spn-kjpaw_psl.0.2.UPF, which are provided in the package.

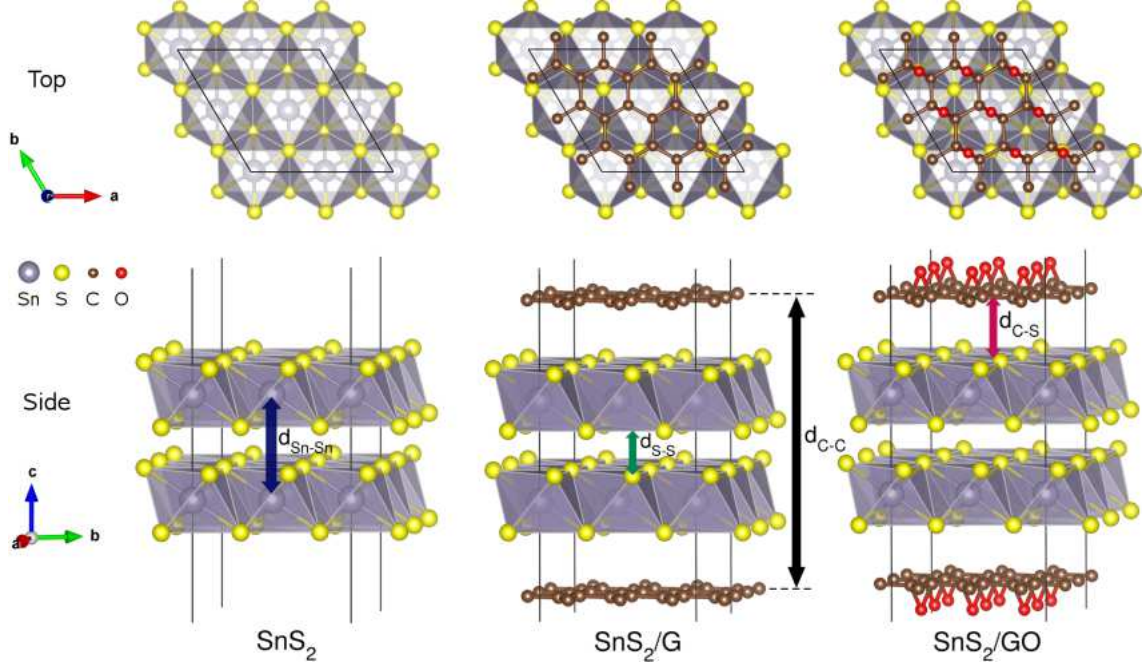


Figure 1: Polyhedral view of relaxed atomic structures of SnS_2 bilayer and hybrid SnS_2/G and SnS_2/GO composites. The hybrid composites contain the two equivalent hetero-interfaces between the SnS_2 and graphene or GO layer. Various interlayer distances are denoted.

the supercell is scarcely changed and the interaction between the layers becomes negligible.

The possibility of interface formation can be estimated by calculating the formation energy per unit area defined as,

$$E_f = \frac{1}{2A} [E_{\text{SnS}_2/\text{G}(\text{GO})} - (N_{\text{SnS}_2} E_{\text{SnS}_2}^{\text{bulk}} + N_{\text{G}(\text{GO})} E_{\text{G}(\text{GO})})] \quad (2)$$

where $E_{\text{SnS}_2/\text{G}(\text{GO})}$ and $E_{\text{G}(\text{GO})}$ are the total energies of the supercells including the hybrid SnS_2/G (GO) bilayer and graphene (GO) monolayer, and $E_{\text{SnS}_2}^{\text{bulk}}$ is the total energy per formula unit of unit cell of the crystalline SnS_2 bulk. N_{SnS_2} and $N_{\text{G}(\text{GO})}$ are the numbers of SnS_2 formula units included in the layer and of the graphene (GO) monolayers, and A is the interfacial area in x - y plane. Since the supercell models include two equivalent interfaces between the SnS_2 and graphene or GO layers as can be seen in Figure 1, the energy difference should be divided by 2 to give the formation energy of the interface.

To estimate the stability of sodium-intercalated compounds, we calculated the sodium intercalation energy E_{int} as follows,

$$E_{\text{int}} = E_{\text{sub+Na}} - (E_{\text{sub}} + E_{\text{Na}}^{\text{bcc}}) \quad (3)$$

where $E_{\text{sub+Na}}$ and E_{sub} are the total energies of the supercells for the sodium intercalated compounds and the pristine substrates (SnS_2 , SnS_2/G and SnS_2/GO), and $E_{\text{Na}}^{\text{bcc}}$ is the total energy per atom of the unit cell of the sodium crystal in body-centered cubic (bcc) phase.

3. Results and Discussion

3.1. Hybrid composites

We first optimized the crystalline structure of SnS_2 bulk in hexagonal phase ($P\bar{3}m1$ space group, see Figure S1) by use of different XC functionals. In accordance with the previous first-principles calculations [43, 44, 45, 46], the PBEsol functional yielded slightly overestimated lattice constants (0.05% and 2% for a and c) while adding the vdW energy in the flavor of Grimme (−0.05% and −5%) or XDM [49] (−0.7% and −5%) gave underestimation, when compared with the experimental values of $a = 3.649 \text{ \AA}$ and $c = 5.899 \text{ \AA}$ [42]. Although XDM gave somewhat severe underestimated interlayer lattice constant for SnS_2 bulk, we choose it for further calculations of interface in this work, based on the established fact that XDM is especially good for modeling of surfaces [51] and organic/inorganic interfaces [52].

Then, we performed atomic relaxations in the supercells of the individual SnS_2 , graphene and GO monolayers, of which 2D x - y planes include (2×2) cells for SnS_2 layer and (3×3) cells for graphene and GO layers (see Figure S1). The cell parameters of these supercells were set to be identical and fixed during the atomic relaxations as $a = b = 7.79 \text{ \AA}$ and $c = 30 \text{ \AA}$, allowing to make a modeling of the hetero-interfaces from these individual layers. In fact, we carried out the variable cell relaxation in only 2D x - y plane of the GO supercell to determine the optimal cell size in the plane. In the graphene and GO layers, the average C–C and C–O bond lengths were determined to be 1.49 and 1.42 \AA , which are comparable with the previous values of 1.51 and 1.42 \AA obtained by first-principles calculations [53, 54, 55].

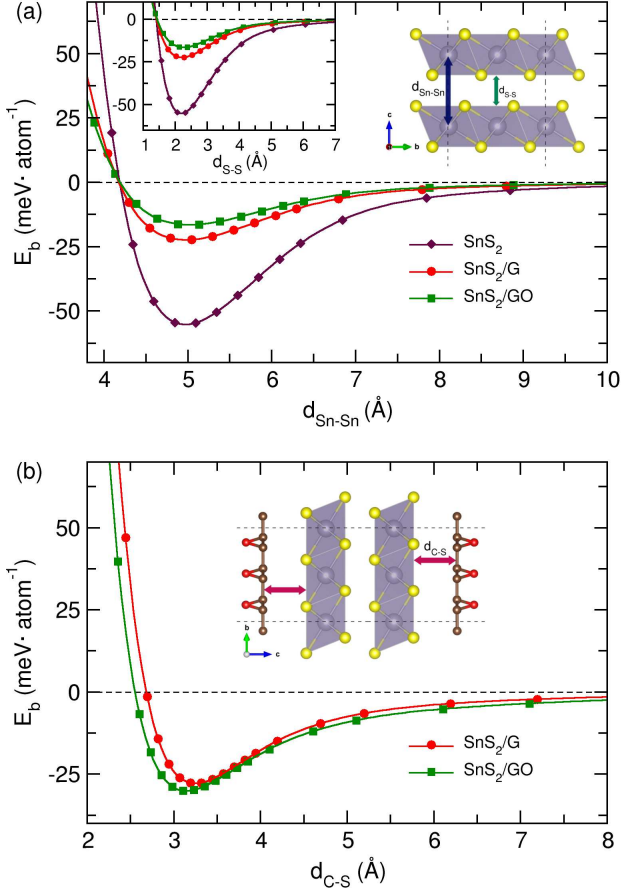


Figure 2: The total energy differences as varying the interlayer distances of (a) $d_{\text{Sn-Sn}}$ and $d_{\text{S-S}}$ (inset) in SnS_2 , SnS_2/G and SnS_2/GO bilayers and (b) $d_{\text{C-S}}$ in SnS_2/G and SnS_2/GO bilayers.

Using these monolayers of SnS_2 , graphene and GO, we made the supercells for SnS_2 bilayer and hybrid SnS_2/G and SnS_2/GO composites with the same sizes to the monolayer supercells, and performed the atomic relaxations to determine the real atomic positions as shown in Figure 1. In these bilayers, the average Sn–S bond lengths were found to be 2.63 Å, which is a little larger than that of 2.56 Å in the bulk, while C–C and C–O bond lengths were almost same to the monolayers due to the same sizes of the supercells.

In order to determine the optimal interlayer distance and the corresponding binding energy between the layers, we estimated the total energy differences of the supercells as varying the interlayer distance. In accordance with the variation of interlayer distance, the supercell length c was also varied to preserve the vacuum layer thickness as 15 Å. Two different interlayer bindings can be distinguished as those between the neighboring SnS_2 layers (homo-interface) and between the SnS_2 and graphene or GO layers (hetero-interface), while four different interlayer distances can be thought as $d_{\text{Sn-Sn}}$, $d_{\text{S-S}}$, $d_{\text{C-S}}$ and $d_{\text{C-C}}$ as depicted in Figure 1. Over the interlayer distance of ~ 15 Å, total energies of the supercells were confirmed to be almost unchangeable, indicating a non-interaction or no binding between the layers. Figure 2 shows the total energy differences

Table 1: Interlayer distance (d), interlayer binding energy per atom (E_b) and interface formation energy (E_f) in SnS_2 , SnS_2/G and SnS_2/GO bilayers.

	SnS_2	SnS_2/G	SnS_2/GO
$d_{\text{Sn-Sn}}$ (Å)	4.97	5.04	5.13
$d_{\text{S-S}}$ (Å)	2.18	2.28	2.37
E_b (SnS_2 – SnS_2) (meV)	–54	–22	–16
$d_{\text{C-S}}$ (Å)		3.19	3.10
E_b (C– SnS_2) (meV)		–28	–30
$d_{\text{C-C}}$ (Å)		13.96	13.87
E_f (J/m ²)	0.81	0.34	0.13

of supercells as functions of interlayer distance in reference to the total energy of supercell with the interlayer distance of ~ 15 Å.

Table 1 lists the determined optimal interlayer distances and binding energies, and interface formation energies. The Sn–Sn and S–S interlayer distances were found to become longer upon the formation of hybrid interfaces from 4.97 and 2.18 Å in SnS_2 bilayer to 5.04 and 2.28 Å in SnS_2/G , and to 5.13 and 2.37 Å in SnS_2/GO . This indicates that there is an attractive interaction between SnS_2 layer and graphene or GO layer, and the strength of SnS_2 –GO interaction can be said to be higher than that of SnS_2 –G interaction due to further lengthening of $d_{\text{Sn-Sn}}$ or $d_{\text{S-S}}$ in the case of GO hybrid. Accordingly, the corresponding interlayer binding energy per atom between the neighboring SnS_2 layers, E_b (SnS_2 – SnS_2), also decreases in magnitude from –54 meV in SnS_2 to –22 meV in SnS_2/G , and to –16 meV in SnS_2/GO . In the cases of hybrid composites of SnS_2/G and SnS_2/GO , the interlayer distance $d_{\text{C-S}}$ in the GO hybrid (3.10 Å) was determined to be shorter than that in the graphene hybrid (3.19 Å), while the binding energy of SnS_2 layer with the GO layer (–30 meV) was found to be higher in magnitude than that with the graphene layer (–28 meV). These also indicate that oxidation of graphene can enhance the interaction between the SnS_2 layer and the graphene layer. It is worth noting that all the calculated interlayer binding energies are smaller than the binding energy between the graphene layers in graphite (–77 meV by PBE+vdW calculation [20, 21]), and all the negative values indicate certain formations of stable interface systems from the individual monolayers.

The interlayer distances between the graphene layers ($d_{\text{C-C}}$) in the hybrid SnS_2/G and SnS_2/GO composites were calculated to be 13.96 and 13.87 Å, indicating that the epoxy groups of GO leads to a contraction of the total interlayer distance. The calculated formation energies of the interfaces from the SnS_2 bulk and graphene or GO monolayer were turned out to be positive, suggesting an endothermic feature of the interface formations. And it can be said from the magnitudes of their formation energies that the hetero-interface in SnS_2/G or SnS_2/GO is easier to form than the homo-interface in SnS_2 , and of the two hetero-interfaces the SnS_2/GO is easier than the SnS_2/G .

3.2. Sodium intercalation and migration

To study the sodium intercalation into these SnS_2 composites containing the interfaces, we considered two different scenarios: (1) sodium intercalation into the middle interspace between

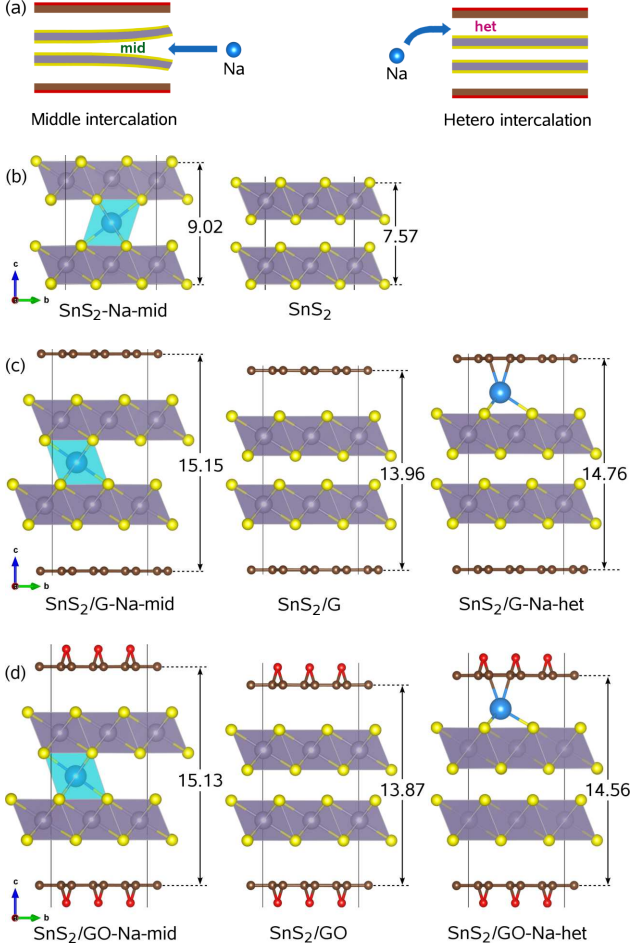


Figure 3: (a) Schematic illustration of sodium intercalation into the middle and hetero interspaces of SnS₂ and graphene or GO composites. Side views of relaxed atomic structures of sodium intercalated (b) SnS₂, (c) SnS₂/G, and (d) SnS₂/GO compounds. Left panel is for the Na middle intercalations, central panel for the substrates, and right panel for the Na hetero intercalations. Typical interlayer distances in Å unit are denoted for comparison.

the neighboring SnS₂ layers, forming *substrate-Na-mid* compounds, and (2) sodium insertion into the hetero interspace between the SnS₂ and graphene or GO layers, forming *substrate-Na-het* compounds, as illustrated in Figure 3(a). For the case of SnS₂ bilayer, only the middle intercalation is surely possible.

In each way of sodium intercalation, we identified the energetically favorable anchoring site of sodium atom by comparing the total energies of the supercells with different sodium insertion sites. In the cases of middle intercalation, two different sites might be thought: (1) Na atom can sit on the top of S atom of the below SnS₂ layer while at the center of S-triangle of the upper SnS₂ layer, leading to a formation of NaS₄ tetrahedron (*tet* site), and (3) Na atom can be placed at the spherical center of SnS₆ octahedron (*oct* site). In energetics the Na middle-intercalated SnS₂ supercell in the *tet* site was found to be about 0.39 eV higher than that in the *oct* site, possibly due to a stronger bonding of Na atom with the surrounding S atoms (see Figure S2). Henceforth, only the *oct* site will be considered for the middle intercalations. Furthermore, it was observed

for the cases of hybrid SnS₂/G (GO) composites that the SnS₂ layers can be shifted in opposite way each other, resulting in the change of layer stacking from AA to AB with a lowering of total energy as 0.21 eV (0.17 eV) (see Figure S2). On the other hand, we distinguished three different sites for the sodium hetero-intercalations in the cases of SnS₂/G (GO) composites: (1) Na atom can sit on the top of Sn atom placed at the center of S-triangle in the below SnS₂ layer while on the side of C–C bond of the upper graphene (GO) layer (*top* site), (2) on the hollow site at the center of S-triangle in the below layer (*hollow* site), and (3) at the center of carbon hexagon ring of the upper layer (*center* site). Among these sodium hetero-intercalation sites, the *top* site was found to have the lowest total energy (see Figure S3).

Figure 3 shows the relaxed atomic structures of sodium-intercalated SnS₂ and SnS₂/G (GO) composites in the lowest energy configurations. It is clear that the volume expansion ratio between the Na-intercalated composite (V_{int}) and the substrate (V_0), $r = \frac{V_{\text{int}}}{V_0} \times 100\%$, which can be readily estimated by using the outermost interlayer distances due to the same in-plane surface area, is distinctly larger in the non-hybrid SnS₂ bilayer (~119%) than in the hybrid SnS₂/G (GO) composites. This indicates that the hybrid of SnS₂ with graphene or GO can effectively reduce the big volume change of SnS₂ itself upon de-/sodiation process. For the both cases of hybrid SnS₂/G and SnS₂/GO composites, meanwhile, the volume expansion ratios upon Na middle intercalations (109%) are larger than the hetero intercalations (105%). As presented in Table 2, the interlayer distances such as $d_{\text{Sn-Sn}}$, $d_{\text{S-S}}$ and $d_{\text{C-C}}$ are clearly smaller in the Na hetero-intercalated compounds than in the middle-intercalated ones. From these results, the sodium intercalation into the hetero-interface between the SnS₂ layer and graphene or GO layer is more profitable for SIB application than into the homo-interface with respect to the volume change. The intercalation energies were calculated to be negative, indicating an exothermic reaction of sodium intercalation from the bilayer substrate and sodium metal. The magnitude of the intercalation energy for the cases of hetero-interfaces was smaller than for the homo-interface, giving an expectation of good performance of Na hetero-intercalated SnS₂/G (GO) as anode materials, which need to possess an electrode potential as low as possible.

We then investigated the diffusion of sodium atom by calculating their activation barriers, which can give a suggestion of

Table 2: Overview of sodium intercalation and diffusion in the both middle and hetero ways, including the interlayer distances d , the volume expansion ratio r , the sodium intercalation energy E_{int} and the sodium migration energy E_{mig} .

	SnS ₂	SnS ₂ /G		SnS ₂ /GO	
	mid	mid	het	mid	het
$d_{\text{Sn-Sn}}$ (Å)	6.21	5.91	4.86	6.02	4.93
$d_{\text{S-S}}$ (Å)	3.37	3.09	2.10	3.19	2.17
$d_{\text{C-S}}$ (Å)		3.26	3.87	3.19	3.65
$d_{\text{C-C}}$ (Å)		15.15	14.76	15.13	14.56
r (%)	119	109	106	109	105
E_{int} (eV)	-0.30	-1.29	-0.76	-1.12	-0.35
E_{mig} (eV)	0.52	0.37	0.32	0.48	0.38

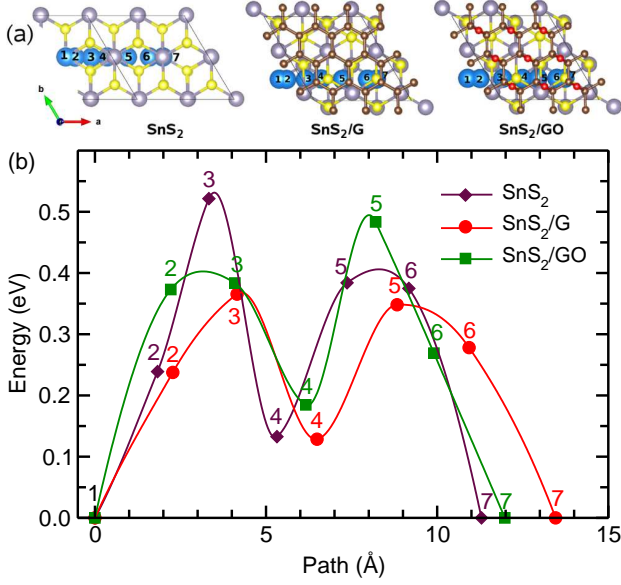


Figure 4: (a) Top view of sodium migrations along the 1D lines within the middle interspaces of SnS₂, SnS₂/G and SnS₂/GO composites, and (b) the corresponding path energy profiles.

the rate capability and cycling stability of electrode materials in SIB application. For the cases of middle intercalation, we considered the sodium migration path from the site determined by atomic relaxation to the adjacent image site, which consists of 7 NEB image configurations. It should be noted that the interval of the neighboring image points was set to be around 1 Å, and the migration paths were determined to be almost straight line along the *a* direction on the *x-y* plane, as shown in Figure 4(a). In Figure 4(b), we show the path energy profile corresponding to the migration paths, from which the activation energy barriers were determined to be 0.52, 0.37 and 0.48 eV for the case of SnS₂, SnS₂/G and SnS₂/GO, respectively. Due to the lower activation energies in the hybrid SnS₂/G or GO composites than in the pristine SnS₂ itself, it can be said that the hybrid of SnS₂ with graphene or GO layer can facilitate the diffusion of sodium.

Figure 5 presents the results of the sodium migration within the hetero-interface between the SnS₂ and graphene or GO layer. We used 5 NEB image configurations due to the shorter length of path. As shown in Figure 5(a), the migration paths are 2D on the *x-y* plane, passing the *top*, *hollow* and *center* sites, as described above subsection. In Figure 5(b), we show the path energy profiles in the hybrid SnS₂/G and SnS₂/GO composites, and the activation barriers as 0.32 and 0.38 eV, which are clearly lower than the corresponding sodium migrations within the middle interface. The migration barriers are also listed in Table 2. To sum up, the sodium atom can migrate more smoothly in the hetero-interspace than in the middle-interspace, and hybrid with graphene is slightly more beneficial than with graphene oxide. It is worth noting that the calculated activation energies are comparable with those for sodium or lithium migration in graphite (0.40 eV) [56] and for sodium-molecule

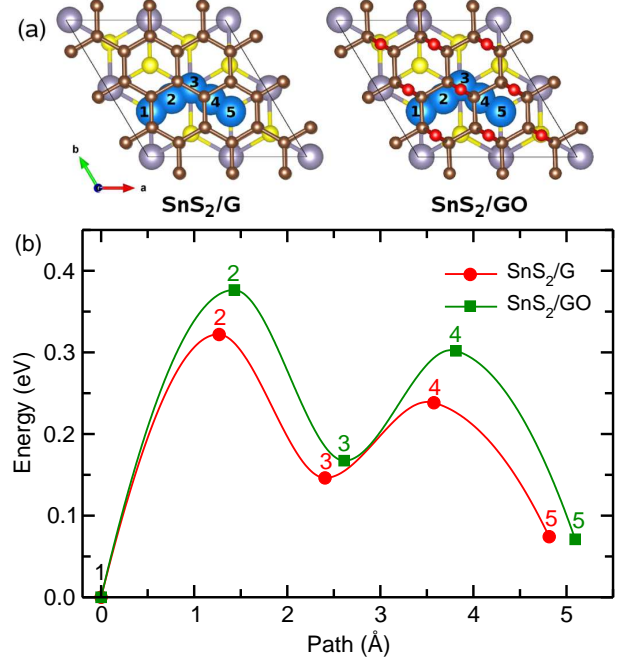


Figure 5: (a) Top view of sodium migrations within the hetero interspaces of hybrid SnS₂/G and SnS₂/GO composites, and (b) the corresponding path energy profiles.

migration (0.40 eV) [20].

3.3. Electronic properties

To further understand such enhancement of sodium insertion by hybrid of SnS₂ with graphene or GO and make it clear the role of hetero-interface, we carried out the analysis of electronic properties such as density of state (DOS) and electronic charge density differences. Such electronic properties can provide us valuable insight for the interaction between the layers and charge transfer in the event of hetero-interface formation, which can be useful for understanding the enhancement of electrochemical properties in the 2D hybrid materials. To obtain an intuitive insight for charge transfer between SnS₂ and graphene or GO layers during the interface formation, we calculated the electronic charge density difference ($\Delta\rho$) as follows,

$$\Delta\rho = \rho_{\text{SnS}_2/\text{G}(\text{GO})} - (\rho_{\text{SnS}_2} + \rho_{\text{G}(\text{GO})}) \quad (4)$$

where $\rho_{\text{SnS}_2/\text{G}(\text{GO})}$, ρ_{SnS_2} and $\rho_{\text{G}(\text{GO})}$ are the charge densities of the hybrid composites, individual SnS₂ and graphene or GO layers, respectively.

In Figure 6, we show the isosurface plot of the electronic charge density differences in the hybrid SnS₂/G and SnS₂/GO composites at the value of ± 0.0005 and $\pm 0.0013 \text{ |e|}\cdot\text{\AA}^{-3}$, respectively. For the case of hybrid SnS₂/G composite, it is shown that the carbon atoms of graphene layer lose some electrons as represented by green-colored charge depletion, while the tin atoms gain the electrons as represented by brown-colored charge accumulation (Figure 6(b) left panel). In Figure 6(c) for the hybrid SnS₂/GO composite, we can also see the electronic charge accumulation around the oxygen atoms as well as the tin atoms,

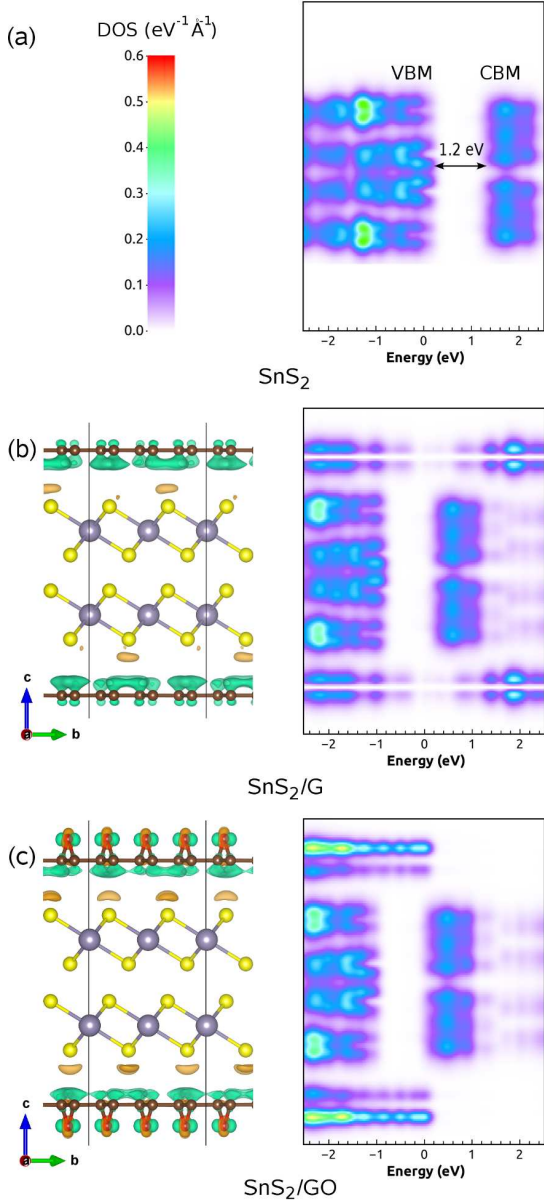


Figure 6: Isosurface plot of electronic charge density differences (left panel) and integrated local density of state (right panel) in (a) SnS₂ bilayer, (b) SnS₂/G and (c) SnS₂/GO composites. The isosurface values are $\pm 0.0005 \text{ |e|} \cdot \text{\AA}^{-3}$ in (b) SnS₂/G and $\pm 0.0013 \text{ |e|} \cdot \text{\AA}^{-3}$ in (c) SnS₂/GO. Brown (green) color represents the electron accumulation (loss). The Fermi level is set to be zero.

while the charge depletion can be seen around the carbon atoms of GO layer as well. In these hybrid composites, therefore, it is clear that the carbon atoms play as electron donors, whereas the tin and oxygen atoms play as electron acceptors, indicating the strong interaction between the SnS₂ layer and graphene or GO layer and thus stable formation of the hetero-interfaces. Due to the influence of oxygen atoms of epoxy groups in the GO hybrid, the extent of charge transfer from the carbon atoms to the oxygen and tin atoms seems to be enhanced compared with the graphene hybrid, leading to the slight strengthening of interlayer interaction between the GO and SnS₂ layers. When

intercalating the Na atom into the bilayerd substrates, the Na and Sn atoms were found to give electrons, leading to the enhanced interaction between the layers (see Figure S4).

We present the local density of state (LDOS) integrated on x - y plane and thus along the z axis in the right panel of Figure 6, where the Fermi level is set to be zero. As shown in Figure 6(a), the SnS₂ bilayer model was found to have a band gap of ~1.2 eV between the valence-band maximum (VBM) and the conduction-band minimum (CBM), which is smaller than that of bulk (2.28 eV) [44], indicating a semiconducting feature of SnS₂ bilayer. In the right panel of Figure 6(b) and (c) for the hybrid cases, however, the Fermi level can be seen to be very close to the CBM belonged to the SnS₂ layer, resulting in an enhancement of electronic conductivity upon hybrid of SnS₂ with graphene or GO. Moreover, we can see the occupied valence states of graphene layer and denser LDOS of GO layer close to the Fermi level in these hybrids, indicating a good in-plane electronic conductivity due to the p_z electron states as already well known before [19, 20, 21]. If the sodium atom intercalated into the hetero-interface, the SnS₂ layers get fill their unoccupied states by the injected electrons from the sodium atom, and thus the Fermi level is placed on the CBM (see Figure S4). These reveal the enhancement of electrochemical properties of the hybrid SnS₂/G (GO) composites compared to the pristine SnS₂ bilayer by formation of hetero-interface through the electron transfer from the graphene or GO layer to the SnS₂ layer.

4. Conclusions

In this work we provide a valuable understanding of material properties of 2D hybrid composites composed of SnS₂ and graphene or GO layers that can be used as effective anode materials of sodium-ion battery. Various supercell models of the pristine SnS₂ bilayer and the hybrid SnS₂/G or GO composites have been suggested, and their atomic structures and energetics were investigated by using first-principles calculations. Through the analysis of the calculated interlayer distances and binding and formation energies, it was revealed that the hetero-interface between the SnS₂ layer and graphene or GO layer can be formed, while oxidation of graphene can enhance the interaction between the layers. Furthermore, we have devised two different models for sodium intercalation such as middle intercalation into the interspace between the SnS₂ layers and hetero intercalation into the interspace between the SnS₂ and graphene or GO layers, and it was found that the hetero-intercalation is more probable due to higher intercalation energy, lower migration energy and smaller volume change. To gain a deep understanding of material properties of these 2D composites, the electronic charge density differences and integrated local density of state were investigated, demonstrating the electron transfer from the graphene layer to the SnS₂ layer and the improvement of electronic conduction by formation of hybrid composites. In conclusion, the 2D hybrid SnS₂/G or GO composite including the hetero-interface can be a promising candidate for anode material of sodium-ion battery.

Associated Content

Supporting Information

The Supporting Information is available free of charge on the ACS Publications website at DOI: xxx/xxx.

Author information

Corresponding Author

*E-mail: cj.yu@ryongnamsan.edu.kp (Chol-Jun Yu)

ORCID

Chol-Jun Yu: 0000-0001-9523-4325

Notes

The authors declare no competing financial interest.

Acknowledgments

This work is supported as part of the fundamental research project “Design of Innovative Functional Materials for Energy and Environmental Application” (No. 2016-20) funded by the State Committee of Science and Technology, DPR Korea. Computation has done on the HP Blade System C7000 (HP BL460c) that is owned by Faculty of Materials Science, Kim Il Sung University.

References

- [1] L. Shi, T. Zhao, Recent advances in inorganic 2D materials and their applications in lithium and sodium batteries, *J. Mater. Chem. A* 5 (2017) DOI: 10.1039/c6ta09831b.
- [2] W. Kang, Y. Wang, J. Xu, Recent progress in layered metal dichalcogenide nanostructures as electrodes for high-performance sodium-ion batteries, *J. Mater. Chem. A* 5 (2017) 7667–7690.
- [3] V. Georgakilas, J. N. Tiwari, K. C. Kemp, J. A. Perman, A. B. Bourlinos, K. S. Kim, R. Zboril, Noncovalent Functionalization of Graphene and Graphene Oxide for Energy Materials, Biosensing, Catalytic, and Biomedical Applications, *Chem. Rev.* 116 (2016) 5464–5519.
- [4] E. Quesnel, F. Roux, F. Emieux, P. Faucherand, E. Kymakis, G. Volonakis, F. Giustino, B. Martin-Garcia, I. Moreels, S. A. Gursel, Graphene-based technologies for energy applications, challenges and perspectives, *2D Mater.* 2 (2015) 030204.
- [5] X. Yu, H. Cheng, M. Zhang, Y. Zhao, L. Qu, G. Shi, Graphene-based smart materials, *Nat. Rev. Mater.* 2 (2017) 17046.
- [6] A. Kaplan, Z. Yuan, J. D. Benck, A. G. Rajan, X. S. Chu, Q. H. Wang, M. S. Strano, Current and future directions in electron transfer chemistry of graphene, *Chem. Soc. Rev.* 46 (2017) 4530–4571.
- [7] A. Ambrosi, C. K. Chua, N. M. Latiff, A. H. Loo, C. H. A. Wong, A. Y. S. Eng, A. Bonanni, M. Pumera, Graphene and its electrochemistry – an update, *Chem. Soc. Rev.* 45 (2016) 2458–2493.
- [8] P. Zhu, B. G. Sumpter, V. Meunier, Electronic, Thermal, and Structural Properties of Graphene Oxide Frameworks, *J. Phys. Chem. C* 117 (2013) 8276–8281.
- [9] S. D. Dabhi, S. D. Gupta, P. K. Jha, Structural, electronic, mechanical, and dynamical properties of graphene oxides: A first principles study, *J. Appl. Phys.* 115 (2014) 203517.
- [10] K. Kubota, N. Yabuuchi, H. Yoshida, M. Dahbi, S. Komaba, Layered oxides as positive electrode materials for Na-ion batteries, *MRS Bull.* 39 (2014) 416–422.
- [11] M. Chhowalla, H. S. Shin, G. Eda, L. J. Li, K. P. Loh, H. Zhang, The chemistry of two-dimensional layered transition metal dichalcogenide nanosheets, *Nat. Chem.* 5 (2013) 263–275.
- [12] M. Pumera, Z. Sofer, A. Ambrosi, Layered transition metal dichalcogenides for electrochemical energy generation and storage, *J. Mater. Chem. A* 2 (2014) 8981–8987.
- [13] M. Naguib, V. N. Mochalin, M. W. Barsoum, Y. Gogotsi, 25th anniversary article: MXenes: a new family of two-dimensional materials, *Adv. Mater.* 26 (2014) 992–2014.
- [14] G. Ali, A. Mehmood, H. Y. Ha, J. Kim, K. Y. Chung, Reduced graphene oxide as a stable and high-capacity cathode material for Na-ion batteries, *Sci. Rep.* 7 (2017) 40910.
- [15] T. Liu, R. Kaviani, I. Kim, S. W. Lee, Self-Assembled, Redox-Active Graphene Electrodes for High-Performance Energy Storage Devices, *J. Phys. Chem. Lett.* 5 (2014) 4324–4330.
- [16] Y.-X. Wang, S.-L. Chou, H.-K. Liu, S.-X. Dou, Reduced graphene oxide with superior cycling stability and rate capability for sodium storage, *Carbon* 57 (2013) 202–208.
- [17] J. Feng, X. Sun, C. Wu, L. Peng, C. Lin, S. Hu, J. Yang, Y. Xie, Metallic Few-Layered VS₂ Ultrathin Nanosheets: High Two-Dimensional Conductivity for In-Plane Supercapacitors, *J. Am. Chem. Soc.* 133 (2011) 17832–17838.
- [18] M. Mortazavi, C. Wang, J. Deng, V. B. Shenoy, N. V. Medhekar, Ab initio characterization of layered MoS₂ as anode for sodium-ion batteries, *J. Power Sources* 268 (2014) 279–286.
- [19] G.-C. Ri, C.-J. Yu, J.-S. Kim, S.-N. Hong, U.-G. Jong, M.-H. Ri, First-principles study of ternary graphite compounds intercalated with alkali atoms (Li, Na, and K) and alkylamines towards alkali ion battery applications, *J. Power Sources* 324 (2016) 758–765.
- [20] C.-J. Yu, S.-B. Ri, S.-H. Choe, G.-C. Ri, Y.-H. Kye, S.-C. Kim, Ab initio study of sodium intercalation with diglyme molecule into graphite, *Electrochim. Acta* 253 (2017) 589–598.
- [21] C.-J. Yu, U.-S. Ri, G.-C. Ri, J.-S. Kim, Revealing the formation and electrochemical properties of bis(trifluoromethanesulfonyl) imide intercalated graphite with first-principles calculations, *Phys. Chem. Chem. Phys.* 20 (2018) 14124–14132.
- [22] D. Lin, Y. Liu, Z. Ling, H. W. Lee, J. Sau, M. Wang, K. Yan, J. Xie, Y. Cui, Layered reduced graphene oxide with nanoscale interlayer gaps as a stable host for lithium metal anodes, *Nat. Nanotechnol.* 11 (2016) 626–632.
- [23] F. Bonaccorso, L. Colombo, G. Yu, M. Stoller, V. Tozzii, A. C. Ferrari, D. S. Ruoff, V. Pellegrini, Graphene, related two-dimensional crystals, and hybrid systems for energy conversion and storage, *Science* 347 (2015) 1246501.
- [24] T.-J. Kim, C. Kim, D. Son, M. Choi, B. Park, Novel SnS₂-nanosheet anodes for lithium-ion batteries, *J. Power Sources* 167 (2007) 529.
- [25] J.-W. Seo, J.-T. Jang, S.-W. Park, C. Kim, B. Park, J. Cheon, Two-Dimensional SnS₂ Nanoplates with Extraordinary High Discharge Capacity for Lithium Ion Batteries, *Adv. Mater.* 20 (2008) 4269–4273.
- [26] H. Zhong, G. Yang, H. Song, Q. Liao, H. Cui, P. Shen, C.-X. Wang, Vertically aligned graphene-like SnS₂ ultrathin nanosheet arrays: Excellent energy storage, catalysis, photo-conduction, and field-emitting performances, *J. Phys. Chem. C* 116 (2012) 9319.
- [27] J. W. Wang, X. H. Liu, S. X. Mao, J. Y. Huang, Microstructural Evolution of Tin Nanoparticles during In Situ Sodium Insertion and Extraction, *Nano Lett.* 12 (2012) 5897–5902.
- [28] L. D. Ellis, T. D. Hatchard, M. N. Obrovac, Reversible Insertion of Sodium in Tin, *J. Electrochem. Soc.* 159 (2012) A1801–A1805.
- [29] E. Pomerantseva, Y. Gogotsi, Two-dimensional heterostructures for energy storage, *Nature Energy* 2 (2017) 17089.
- [30] H. Chauhan, K. Soni, M. Kumar, S. Deka, Tandem Photocatalysis of Graphene-Stacked SnS₂ Nanodiscs and Nanosheets with Efficient Carrier Separation, *ACS Omega* 1 (2016) 127–137.
- [31] Q. Pan, J. Xie, T. Zhu, G. Cao, X. Zhao, S. Zhang, Reduced Graphene Oxide-Induced Recrystallization of NiS Nanorods to Nanosheets and the Improved Na-Storage Properties, *Inorg. Chem.* 53 (2014) 3511–3518.
- [32] L. Zhou, X. Kong, M. Gao, F. Lian, B. Li, Z. Zhou, H. Cao, Hydrothermal Fabrication of MnCO₃@rGO Composite as an Anode Material for High-Performance Lithium Ion Batteries, *Inorg. Chem.* 53 (2014) 9228–9234.
- [33] A. K. Geim, I. V. Grigorieva, Van der Waals heterostructures, *Nature* 499 (2013) 419–425.
- [34] L. David, R. Bhandavat, G. Singh, MoS₂/graphene composite paper for sodium-ion battery electrodes, *ACS Nano* 8 (2014) 1759–1770.
- [35] X. Xie, Z. Ao, D. Su, J. Zhang, G. Wang, MoS₂/graphene composite anodes with enhanced performance for sodium-ion batteries: the role of the two dimensional heterointerface, *Adv. Funct. Mater.* 25 (2015) 1393–1403.

- [36] K. Chang, Z. Wang, G. Huang, H. Li, W. Chen, J. Y. Lee, Few-layer SnS_2 /graphene hybrid with exceptional electrochemical performance as lithium-ion battery anode, *J. Power Sources* 201 (2011) 259–266.
- [37] C. Ma, J. Xu, J. Alvarado, B. Qu, J. Somerville, J. Y. Lee, Y. S. Meng, Investigating the Energy Storage Mechanism of SnS_2 -rGO Composite Anode for Advanced Na-Ion Batteries, *Chem. Mater.* 27 (2015) 5633–5640.
- [38] B. Qu, C. Ma, G. Ji, C. Xu, J. Xu, Y. S. Meng, T. Wang, J. Y. Lee, Layered SnS_2 -Reduced Graphene Oxide Composite – A High-Capacity, High-Rate, and Long-Cycle Life Sodium-Ion Battery Anode Material, *Adv. Mater.* 26 (2014) 3854–3859.
- [39] Y. Zhang, P. Zhu, L. Huang, J. Xie, S. Zhang, G. Cao, X. Zhao, Few-Layered SnS_2 on Few-Layered Reduced Graphene Oxide as Na-Ion Battery Anode with Ultralong Cycle Life and Superior Rate Capability, *Adv. Funct. Mater.* 25 (2015) 481–489.
- [40] W. Xu, K. Zhao, L. Zhang, Z. Xie, Z. Cai, Y. Wang, SnS_2 @Graphene nanosheet arrays grown on carbon cloth as freestanding binder-free flexible anodes for advanced sodium batteries, *J. Alloys Compounds* 654 (2016) 357–362.
- [41] B. Luo, Y. Fang, B. Wang, J. Zhou, H. Song, L. Zhi, Two dimensional graphene- SnS_2 hybrids with superior rate capability for lithium ion storage, *Energy Environ. Sci.* 5 (2012) 5226.
- [42] L. A. Burton, T. J. Whittles, D. Hesp, W. M. Linhart, J. M. Skelton, B. Hou, R. F. Webster, G. O'Dowd, C. Reece, D. Cherns, D. J. Fermin, T. D. Veal, V. R. Dhanak, A. Walsh, Electronic and optical properties of single crystal SnS_2 : An earth-abundant disulfide photocatalyst, *J. Mater. Chem. A* 4 (2016) 1312.
- [43] Y. Kumagai, L. A. Burton, A. Walsh, F. Oba, Electronic Structure and Defect Physics of Tin Sulfides: SnS , Sn_2S_3 , and SnS_2 , *Phys. Rev. Appl.* 6 (2016) 014009.
- [44] T. J. Whittles, L. A. Burton, J. M. Skelton, A. Walsh, T. D. Veal, V. R. Dhanak, Band Alignments, Valence Bands, and Core Levels in the Tin Sulfides SnS , SnS_2 , and Sn_2S_3 : Experiment and Theory, *Chem. Mater.* 28 (2016) 3718–3726.
- [45] J. M. Skelton, L. A. Burton, F. Oba, A. Walsh, Chemical and Lattice Stability of the Tin Sulfides, *J. Phys. Chem. C* 121 (2017) 6446–6454.
- [46] J. M. Skelton, L. A. Burton, A. J. Jackson, F. Oba, S. C. Parker, A. Walsh, Lattice dynamics of the tin sulphides SnS_2 , SnS and Sn_2S_3 : vibrational spectra and thermal transport, *Phys. Chem. Chem. Phys.* 19 (2017) 12452–12465.
- [47] P. Giannozzi, S. Baroni, N. Bonini, M. Calandra and R. Car, et al., QUANTUM ESPRESSO: a modular and open-source software project for quantum simulations of materials, *J. Phys.: Condens. Matter* 21 (2009) 395502.
- [48] J. P. Perdew, A. Ruzsinszky, G. I. Csonka, O. A. Vydrov, G. E. Scuseria, L. A. Constantin, X. Zhou, K. Burke, Restoring the Density Gradient Expansion for Exchange in Solids and Surfaces, *Phys. Rev. Lett.* 100 (2008) 136406.
- [49] A. O. de la Roza, E. R. Johnson, Many-body dispersion interaction from the exchange-hole dipole moment model, *J. Chem. Phys.* 138 (2013) 054103.
- [50] G. Henkelman, B. P. Uberuaga, H. Jónsson, A climbing image nudged elastic band method for finding saddle points and minimum energy paths, *J. Chem. Phys.* 113 (2000) 9901–9904.
- [51] S.-N. Hong, Y.-H. Kye, C.-J. Yu, U.-G. Jong, G.-C. Ri, C.-S. Choe, K.-H. Kim, J.-M. Han, Ab initio thermodynamic study of the SnO_2 (110) surface in an O_2 and NO environment: a fundamental understanding of the gas sensing mechanism for NO and NO_2 , *Phys. Chem. Chem. Phys.* 18 (2016) 31566–31578.
- [52] E. R. Johnson, *Non-covalent Interactions in Quantum Chemistry and Physics*, Elsevier, 2017.
- [53] Z. Šljivančanin, A. S. Milošević, Z. S. Popović, F. R. Vukajlović, Binding of atomic oxygen on graphene from small epoxy clusters to a fully oxidized surface, *Carbon* 54 (2013) 482–488.
- [54] J.-A. Yan, M. Y. Chou, Oxidation functional groups on graphene: structural and electronic properties, *Phys. Rev. B* 82 (2010) 125403.
- [55] L. Wang, Y. Y. Sun, K. Lee, D. West, Z. F. Chen, J. J. Zhao, S. B. Zhang, Stability of graphene oxide phases from first-principles calculations, *Phys. Rev. B* 82 (2010) 161406(R).
- [56] K. Nobuhara, H. Nakayama, M. Nose, S. Nakanishi, H. Iba, First-principles study of alkali metal-graphite intercalation compounds, *J. Power Sources* 243 (2013) 585–587.